Heat-Exchanger Deposits in an Inverted Steam-Assisted Gravity Drainage Operation. Part 2. Organic Acid Analysis by Electrospray Ionization Fourier Transform Ion Cyclotron Resonance Mass Spectrometry

Tanner M. Schaub,[†] David W. Jennings,[‡] Sunghwan Kim,[†,§] Ryan P. Rodgers,*[,†,||] and Alan G. Marshall*[,†,||]

National High Magnetic Field Laboratory, Florida State University, 1800 East Paul Dirac Drive, Tallahassee, Florida 32310-4005, and Baker Petrolite, 12645 West Airport Boulevard, Sugar Land, Texas 77478

Received March 19, 2006. Revised Manuscript Received October 15, 2006

As a complement to the bulk analyses presented in part 1 (Jennings, D. W.; Shaikh, A. *Energy Fuels* **2007**, *21*, 176−184), we report detailed compositional analysis of the organic acids from heat-exchanger deposits and produced water from an inverted steam-assisted gravity drainage (SAGD) bitumen production process. The current analyses were performed by ultrahigh-resolution negative-ion electrospray ionization Fourier transform ion cyclotron resonance mass spectrometry [(−) ESI FT-ICR MS] and reveal distributions of molecular weight, heteroatom content, aromaticity, and carbon number for several thousand organic acids in each sample. High mass accuracy combined with Kendrick mass defect analysis allows for assignment of a unique elemental composition, $C_cH_hN_nO_oS_s$, to each mass spectral peak. Three-dimensional mass spectral images generated from the molecular formulas reveal compositional differences that may be rationalized on the basis of sample processing. In particular, we report lower overall heteroatom content, higher average carbon number, and lower aromaticity for early stage deposits and the produced bitumen compared to later stage samples that show increased water solubility. Little was previously known about those species other than the presence of organic acid/acid salt functionality. Moreover, we report the first *in vacuo* isolation and tandem mass spectrometry of individual components of petroleum mixtures. Tandem mass spectrometry by infrared multiphoton dissociation of trapped ions indicates dicarboxylic acid structures for predominant $C_cH_hO_4$ and dicarboxylic acid structures with thiophenic sulfur for predominant $C_cH_hSO_4$ species. In this manner, we provide a highly detailed landscape for the organic acid content of inverted SAGD heat-exchanger deposits, to further illuminate the nature of fouling in those systems.

Introduction

A general discussion of heat-exchanger fouling in steam-assisted gravity drainage (SAGD) bitumen production operations is provided in the part 1 companion paper (see Jennings, D. W.; Shaikh, A. *Energy Fuels* **2007**, *21*, 176−184),[1] where the importance of SAGD as a production method for the vast bitumen reserves of Canada is outlined. Here, we focus on the application of ultrahigh-resolution Fourier transform ion cyclotron resonance mass spectrometry (FT-ICR MS) for detailed elemental compositional analysis of heat-exchanger deposits from an inverted SAGD processing facility in Alberta, Canada. The suitability of FT-ICR MS for the analysis of complex petroleum mixtures has recently been reviewed,[2−4] and a variety of petroleum samples have been interrogated with this technique.

Petroleum mixtures are exceedingly compositionally complex, and their mass spectra are the most complex ever observed. For example, more than 12 400 molecular formulas were recently assigned in the range of 280−700 Da for a single negative-ion atmospheric pressure photoionization FT-ICR mass spectrum of a South American crude oil, with as many as 63 resolved peaks in a 0.4 Da spectral segment.[5] For mixtures of such complexity, ultrahigh mass resolving power (e.g., $m/\Delta m_{50\%} > 200\,000$ at m/z 200−1200, in which m is the ion mass and $\Delta m_{50\%}$ is the mass spectral peak full-width at half-maximum peak height) is required to resolve signals for numerous isobaric compounds, including those with elemental compositions that differ by ^{12}CH versus $^{13}C_1$ (4.5 mDa), $^{12}C_3$ versus SH_4 (3.4 mDa), and $^{12}C_4$ versus $^{13}CSH_3$ (1.1 mDa). Resolving power of that magnitude is available only by FT-ICR MS. Once the multitude of ion signals for a given petroleum mixture is

* To whom correspondence should be addressed: Ion Cyclotron Resonance Program, National High Magnetic Field Laboratory, Florida State University, 1800 E. Paul Dirac Dr., Tallahassee, FL 32310-4005. E-mail: marshall@magnet.fsu.edu.

† National High Magnetic Field Laboratory.

‡ Baker Petrolite.

§ Present address: Korean Basic Science Institute, 52 YeoEun-Dong, Yuseong-Gu, Daejeon, Korea.

|| Also a member of the Department of Chemistry and Biochemistry, Florida State University, Tallahassee, FL 32306.

(1) Jennings, D. W.; Shaikh, A. Heat-exchanger deposition in an inverted steam-assisted gravity drainage operation. Part 1. Inorganic and organic analyses of deposit samples. *Energy Fuels* **2007**, *21*, 176−184.

(2) Marshall, A. G.; Hendrickson, C. L.; Shi, S. D. H. Scaling MS plateaus with high-resolution FT-ICRMS. *Anal. Chem.* **2002**, *74*, 252A−259A.

(3) Marshall, A. G.; Rodgers, R. P. Petroleomics: The next grand challenge for chemical analysis. *Acc. Chem. Res.* **2004**, *37*, 53−59.

(4) Rodgers, R. P.; Schaub, T. M.; Marshall, A. G. Petroleomics: MS returns to its roots. *Anal. Chem.* **2005**, *77*, 20A−27A.

(5) Purcell, J. M.; Hendrickson, C. L.; Rodgers, R. P.; Marshall, A. G. In Atmospheric Pressure Photoionization Fourier Transform Ion Cyclotron Resonance Mass Spectrometry for Complete Mixture Analysis. *Anal. Chem.* **2006**, *78*, 5906−5912.

10.1021/ef0601115 CCC: $37.00
Published on Web 01/03/2007

resolved, sub-ppm mass measurement accuracy (also exclusive to FT-ICR MS) provides the capability to explicitly assign elemental composition for ions up to ~400 Da. Kendrick mass sorting[6,7] enables the assignment of higher mass species by identification of homologous series [elemental compositions with a particular heteroatom ($N_nO_oS_s$) composition and double-bond equivalents (DBE, number of rings plus double bonds) but differing by increments of CH_2]. Homologous series are found by converting the measured International Union of Pure and Applied Chemistry (IUPAC) mass to the Kendrick mass [Kendrick mass = IUPAC mass × (14/14.015 65), in which the denominator is the IUPAC mass of a CH_2 unit], followed by sorting the Kendrick masses based on the Kendrick mass defect [Kendrick mass defect = (nominal Kendrick mass − exact Kendrick mass)]. The elemental compositions of higher mass members of each homologous series (greater than ~500 Da) are therefore assigned by tracking the series upward from an accurate mass measurement of the lower mass species.[3]

Various ionization sources have been interfaced to FT-ICR mass analyzers to access the various chemical classes expected from petroleum. For example, electron ionization,[8−11] field desorption ionization,[12,13] atmospheric pressure photoionization,[5] and laser-induced acoustic desorption[14] provide access to nonpolar components of petroleum. Both positive- and negative-ion electrospray are particularly effective for ionizing polar components of those mixtures.[3,4] Although polar compounds represent only a small fraction of the species in petroleum, they are nonetheless important in such critical aspects of petroleum production as corrosion/corrosivity,[15] catalyst deactivation in hydrotreatment processes, and bitumen production.[16]

Here, we apply negative-ion electrospray ionization [(−) ESI] FT-ICR MS to analyze inverted SAGD heat-exchanger deposits and related samples. Because negative-ion electrospray ionizes only acidic polar constituents, basic polar and nonpolar species will not be observed. ESI obviously relies on sample dissolution prior to ionization. Analyses performed on bulk material[1] indicate that organic acid species comprise a significant fraction of the total and are present in both the free acid form and as acid salts. The organic acid salts, however, exhibit very limited solubility in electrospray-compatible solvents, thus precluding their analysis by ESI FT-ICR MS.

Experimental Section

Samples. Nine samples from an operational SAGD reverse-emulsion processor were analyzed: bitumen, six heat-exchanger deposit samples, and two solid samples isolated from produced water that exits the high-temperature separator in the facility. The processing is shown schematically in Figure 1, with sample locations indicated by red text and arrows. Note that the single heat exchangers shown in the diagram are banks of exchangers in the actual facility. Exchanger A is integrated for heat management and uses produced water to heat the incoming reverse emulsion. Exchanger A undergoes deposition on both the reverse-emulsion flow side (shell) and the produced water flow side (tube).

The physical characteristics and bulk inorganic and organic contents of the samples are discussed in the part 1 companion paper.[1] Photographs of heat-exchanger equipment and deposits are also shown in part 1. In the notation of part 1, the heat-exchanger deposit samples analyzed in this paper were A-RE-1, A-RE-2, A-PW-1, A-PW-2, B-PW-1, and C-PW-1. Produced water suspended solids were collected by centrifuging an aliquot of produced water, decanting the water, and air-drying. A produced water acid-precipitated sample was prepared by filtering 40 mL of produced water through a 0.7 μm glass fiber filter into a centrifuge produced water followed by the addition of ~80 μL of concentrated HCl. The sample was allowed to sit overnight, then centrifuged, and water-siphoned. Residual water was then evaporated by placing the sample in a fume hood for 18 h followed by 2 h in a vacuum oven at 90 °C.

Samples were prepared for ESI FT-ICR MS analysis by dissolution of 2 mg of dry sample in 1 mL of toluene followed by the addition of 1 mL of methanol containing ~1% ammonium hydroxide (the base was added to facilitate deprotonation during ESI).

Mass Spectrometry. (−) ESI FT-ICR MS was performed with a home-built 9.4 T FT-ICR mass spectrometer[17,18] as previously described.[19] Briefly, the sample solution is supplied to a micro-electrospray source (−2.5 kV, 500 nL/min) at the inlet of the mass spectrometer. Charged droplet desolvation occurs in a 0.6 mm i.d., 20 cm long heated metal capillary that is followed by a tube lens/skimmer cone. Ions are transported through RF-only octopole and resolving quadrupole ion guides prior to collection in a linear octopole ion trap for 2−10 s. Externally accumulated[20] ions are then injected to a Penning ion trap located in the magnetic field

(6) Hughey, C. A.; Hendrickson, C. L.; Rodgers, R. P.; Marshall, A. G.; Qian, K. Kendrick mass defect spectrum: A compact visual analysis for ultrahigh-resolution broadband mass spectra. *Anal. Chem.* **2001**, *73*, 4676−4681.

(7) Kendrick, E. Mass scale based on CH_2 = 14.0000 for high-resolution mass spectrometry of organic compounds. *Anal. Chem.* **1963**, *35*, 2146−2154.

(8) Fu, J.; Purcell, J. M.; Quinn, J. P.; Schaub, T. M.; Hendrickson, C. L.; Rodgers, R. P.; Marshall, A. G. External ionization 7 T Fourier transform ion cyclotron resonance mass spectrometer for resoluition and identification of volatile organic mixtrues. *Rev. Sci. Instrum.* **2005**, *77*, 025102.

(9) Guan, S.; Marshall, A. G.; Scheppele, S. E. Resolution and chemical formula identification of aromatic hydrocarbons and aromatic compounds containing sulfur, nitrogen, or oxygen in petroleum distillates and refinery streams. *Anal. Chem.* **1996**, *68*, 46−71.

(10) Hsu, C. S.; Liang, Z.; Campana, J. E. Hydrocarbon characterization by ultrahigh resolution FTICRMS. *Anal. Chem.* **1994**, *66*, 850−855.

(11) Rodgers, R. P.; White, F. M.; McIntosh, D. G.; Marshall, A. G. 5.6 T Fourier transform ion cyclotron resonance mass spectrometer for analysis of volatile complex mixtures. *Rev. Sci. Instrum.* **1998**, *69*, 2278−2284.

(12) Schaub, T. M.; Hendrickson, C. L.; Quinn, J. P.; Rodgers, R. P.; Marshall, A. G. Instrumentation and method for ultrahigh resolution field desorption ionization Fourier transform ion cyclotron resonance mass spectrometry of nonpolar species. *Anal. Chem.* **2005**, *77*, 1317−1324.

(13) Schaub, T. M.; Rodgers, R. P.; Marshall, A. G.; Qian, K.; Green, L. A.; Olmstead, W. N. Speciation of aromatic compounds in petroleum refinery streams by continuous flow field desorption ionization FT-ICR mass spectrometry. *Energy Fuels* **2005**, *19*, 1566−1573.

(14) Campbell, J. L.; Crawford, K. E.; Kenttaemaa, H. I. Analysis of saturated hydrocarbons by using chemical ionization combined with laser-induced acoustic desorption/Fourier transform ion cyclotron resonance mass spectrometry. *Anal. Chem.* **2004**, *76*, 959−963.

(15) Klein, G. C.; Rodgers, R. P.; Teixeira, M. A. G.; Teixeira, A. M. R. F.; Marshall, A. G. Petroleomics: Electrospray ionization FT-ICR mass analysis of NSO compounds for correlation between total acid number, corrosivity, and elemental composition. *Prepr. Symp.—Am. Chem. Soc., Div. Fuel Chem.* **2003**, *48*, 14−15.

(16) Rahimi, P.; Rodgers, R.; Marshall, A. G.; Teclemariam, A.; Akbarzadeh, K.; de Bruijn, T. Detailed molecular characterization of naphthenic acids in Athabasca bitumen. *Prepr.—Am. Chem. Soc., Div. Pet. Chem.* **2005**, *50*, 266−268.

(17) Hendrickson, C. L.; Quinn, J. P.; Emmett, M. R.; Marshall, A. G. In *Quadrupole Mass Filtered External Accumulation for Fourier Transform Ion Cyclotron Resonance Mass Spectrometry*, Proceedings of the 48th American Society for Mass Spectromtry Conference on Mass Spectromtry and Allied Topics; American Society for Mass Spectromtry: Long Beach, CA, 2000; p MPB 083.

(18) Senko, M. W.; Hendrickson, C. L.; Pasa-Tolic, L.; Marto, J. A.; White, F. M.; Guan, S.; Marshall, A. G. Electrospray ionization FT-ICR mass spectrometry at 9.4 T. *Rapid Commun. Mass Spectrom.* **1996**, *10*, 1824−1828.

(19) Qian, K.; Rodgers, R. P.; Hendrickson, C. L.; Emmett, M. R.; Marshall, A. G. Reading chemical fine print: Resolution and identification of 3000 nitrogen-containing aromatic compounds from a single electrospray ionization Fourier transform ion cyclotron resonance mass spectrum of heavy petroleum crude oil. *Energy Fuels* **2001**, *15*, 492−498.

(20) Senko, M. W.; Hendrickson, C. L.; Emmett, M. R.; Shi, S. D.-H.; Marshall, A. G. External accumulation of ions for enhanced electrospray ionization Fourier transform ion cyclotron resonance mass spectrometry. *J. Am. Soc. Mass Spectrom.* **1997**, *8*, 970−976.

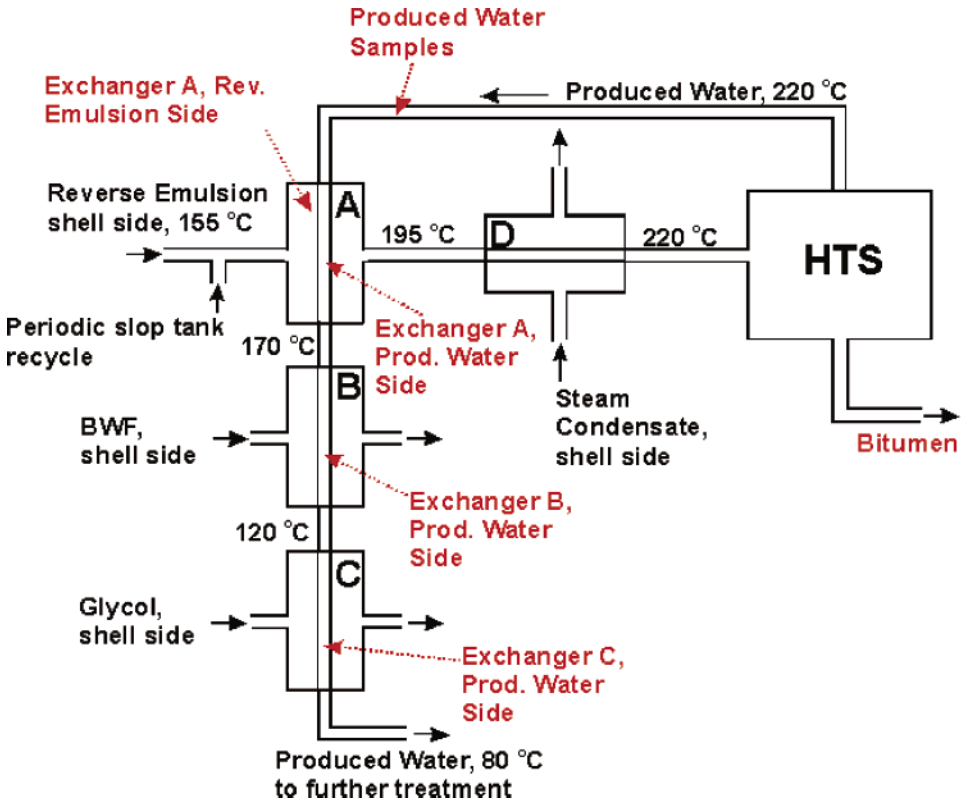

Figure 1. Schematic diagram of the heat exchanger and high-temperature separator (HTS) portion of an inverted SAGD processing facility. Sampling locations are indicated by red text and arrows.

and subjected to swept frequency dipolar excitation (~200 V_{p-p} from 70 to 640 kHz at 150 Hz/μs). The detected signals were digitized (1.2 MHz bandwidth, 4 M time-domain data) and transferred to the control PC. A total of 200 time-domain transients were co-added for each sample and stored for later fast Fourier transformation and frequency−mass conversion.[21,22] The stored time-domain signal was Hanning-apodized and zero-filled once prior to fast Fourier transformation and generation of the magnitude mode frequency domain spectrum. A modular ICR data system (MIDAS) data station, developed in-house, provides instrument control, data acquisition, and data analysis.[23,24]

Data Processing. From the broadband mass spectra, IUPAC masses for singly charged ions with a spectral magnitude greater than 3σ of baseline noise between 225−1000 Da were converted to the Kendrick mass as previously described.[6] The Kendrick mass values were imported to a spreadsheet and sorted on the basis of the Kendrick mass defect. Sorting in this manner allows for identification of homologous series (compounds with a particular heteroatom composition and the same DBE but differing by multiples of CH_2) that are then assigned to molecular formulas. For species less than ~400 Da in mass, ±1 ppm mass accuracy alone suffices for unique molecular formula assignment. For those species (i.e., the lowest mass species of each homologous alkylation series), a molecular formula calculator program limited to molecular compositions with any number of ^{12}C and ^{1}H, up to 3 ^{13}C, 5 ^{15}N, 10 ^{16}O, 5 ^{32}S, and 2 ^{34}S, assigns elemental compositions. Molecular formulas of higher mass members of each homologous alkylation series are then assigned starting from the accurate mass measurement of the lower mass species.

Tandem Mass Spectrometry. Tandem mass spectrometry was performed (with the above-mentioned mass spectrometer) for structural characterization of some of the major species observed in the broadband mass spectra. Specifically, infrared multiphoton dissociation[25] (IRMPD; λ = 10.6 μm, 15−25 W, 150 ms of irradiation, Synrad CO_2 laser, Mukilteo, WA) was performed for O_4, O_2, SO_4, and SO_2 compounds isolated from the broadband ion population. A typical isolation/fragmentation procedure is shown in Figure 2. The complexity of these mixtures necessitates a dual isolation approach prior to IR irradiation. Specifically, a 2−4 Da mass spectral segment is isolated by passing ions through a resolving quadrupole mass filter prior to external ion accumulation,[17] followed by stored waveform inverse Fourier transform (SWIFT) isolation[26−28] in the Penning ion trap to isolate ions in a very narrow mass range prior to infrared irradiation.

Results and Discussion

The ESI FT-ICR MS analyses of samples A-RE-2 and A-PW-2 exhibited results nearly identical to those for samples A-RE-1 and A-PW-1. Thus, we shall discuss only the A-RE-1 and A-PW-1 results. The primary difference between these two sets of similar samples is that they originate from different heat exchangers within the exchanger A bank.

(21) Ledford, E. B., Jr.; Rempel, D. L.; Gross, M. L. Space charge effects in Fourier transform mass spectrometry. Mass calibration. *Anal. Chem.* **1984**, *56*, 2744−2748.

(22) Shi, S. D.-H.; Drader, J. J.; Freitas, M. A.; Hendrickson, C. L.; Marshall, A. G. Comparison and interconversion of the two most common frequency-to-mass calibration functions for Fourier transform ion cyclotron resonance mass spectrometry. *Int. J. Mass Spectrom.* **2000**, *195/196*, 591−598.

(23) Blakney, G. T.; van der Rest, G.; Johnson, J. R.; Freitas, M. A.; Drader, J. J.; Shi, S. D.-H.; Hendrickson, C. L.; Kelleher, N. L.; Marshall, A. G. In *Further Improvements to the MIDAS Data Station for FT-ICR Mass Spectrometry*, Proceedings of the 49th American Society for Mass Spectromtry Conference on Mass Spectromtry and Allied Topics; American Society for Mass Spectromtry: Chicago, IL, May, 2001; p WPM265.

(24) Senko, M. W.; Canterbury, J. D.; Guan, S.; Marshall, A. G. A high-performance modular data system for FT-ICR mass spectrometry. *Rapid Commun. Mass Spectrom.* **1996**, *10*, 1839−1844.

(25) Little, D. P.; Speir, J. P.; Senko, M. W.; O'Connor, P. B.; McLafferty, F. W. Infrared multiphoton dissociation of large multiply charged ions for biomolecule sequencing. *Anal. Chem.* **1994**, *66*, 2809−2815.

(26) Guan, S.; Marshall, A. G. Stored waveform inverse Fourier transform axial excitation/ejection for quadrupole ion trap mass spectrometry. *Anal. Chem.* **1993**, *65*, 1288−1294.

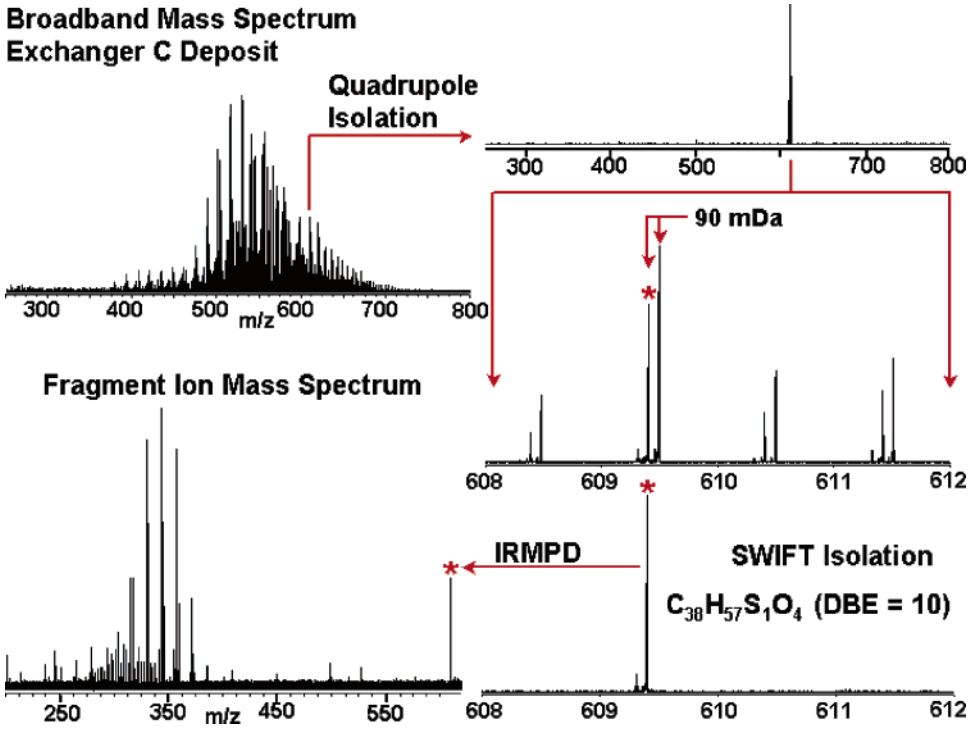

Figure 2. Isolation of ions from a very narrow mass window from a broadband ion population and subsequent fragmentation by infrared photon irradiation. Beginning at the upper left and proceeding clockwise, a narrow mass band including ions of interest is isolated by a quadrupole mass filter prior to ion accumulation. The quadrupole-selected ions are then transferred to a Penning ion trap and subjected to SWIFT[25−27] isolation for more precise separation of the ions of interest. The remaining ions are then IR-irradiated to induce fragmentation, and the fragment ions are detected by FT-ICR MS.

The elemental compositions, $C_cH_hN_nO_oS_s$, derived from high-resolution mass spectra are generally reported at three levels: class analysis to display heteroatom distribution; "type" analysis to reveal the degree of unsaturation for a given class, expressed as DBE (the number of rings plus double bonds, DBE $= c - h/2 + n/2 + 1$); and carbon number distribution (a measure of the degree of alkylation) for each class and type.

Heteroatom Class Analysis. Class analyses are shown in Figure 3. Note that half of the classes (those with the lowest relative abundances) have been omitted for simplicity. Ionization efficiencies/response factors are unavailable for the reported compound types.

The class distributions fall into two general groups: bitumen-like samples and produced water samples. The bitumen-like samples (group 1) include the bitumen and the deposits from both the produced water (A-PW-1) and reverse-emulsion sides (A-RE-1) of exchanger A. The produced water samples (group 2) include the suspended solids from the produced water, the acid-precipitated solids from the produced water, and the produced water-side deposits from exchangers B (B-PW-1) and C (C-PW-1). Generally, species that contain high numbers of heteroatoms were observed at elevated abundances in all group 2 samples (especially O_4 and SO_4 compounds). No SO_4 compounds were observed in the bitumen. Although exchanger A produced water-side deposit originates from the produced water, class analysis for the former appears most like the bitumen and reverse-emulsion deposit samples. The exchanger A produced water-side deposit originates from the first exchanger downstream of the high-temperature separator and may be expected to contain more bitumen/reverse-emulsion-like species because of carryover. In fact, bulk analyses[1] indicate carryover and deposition of inorganic material from the high-temperature separator into the produced water side of exchanger A. Also, from bulk analysis, continued deposition of inorganic material is dramatically reduced in exchangers B and C, indicating that most of the carryover material deposits in exchanger A.

The group 1 samples contain high relative abundances of O_2, O_2S_1, and N_1 compounds relative to group 2. The high relative abundance of O_4, SO_4, and other high heteroatom content compounds for group 2 is likely due to their higher water solubility and/or greater ability to be dispersed in water because of additional oxygen atoms. The produced water acid-precipitated sample in particular shows a marked increase in highly oxygenated compounds especially O_4-O_8 compounds (some data not shown). Classes omitted from Figure 2 include O_1S_1, O_2S_3, and O_7 (observed in both groups 1 and 2), O_1, N_3O_1, and N_1S_1 (observed in group 1 samples only), and O_3S_2, O_7S_1, O_8, and N_1O_5 (observed in group 2 samples only). Notable among those classes is a relatively high abundance of O_1 compounds in the bitumen, relatively high abundance of N_1S_1 compounds in all group 1 samples, and O_7S_1 compounds observed at ~1.5% relative abundance in the produced water acid-precipitated sample.

Type and Carbon Number Distributions: Three-Dimensional Mass Spectral Images. A convenient method for simultaneous visualization of type and carbon number distributions for a given class is to plot DBE versus the carbon number with the relative abundance (color-coded) in the third dimension. Those plots illustrate interclass compositional variation. At this point, it is worth noting that a modest shift in such a distribution

(27) Marshall, A. G.; Wang, T. C.; Ricca, T. L. Tailored excitation for Fourier transform ion cyclotron mass spectrometry. *J. Am. Chem. Soc.* **1985**, *107*, 7893−7897.

(28) Wang, T. C. L.; Ricca, T. L.; Marshall, A. G. Extension of dynamic range in Fourier transform ion cyclotron resonance mass spectrometry via stored waveform inverse Fourier transform excitation. *Anal. Chem.* **1986**, *58*, 2935−2938.

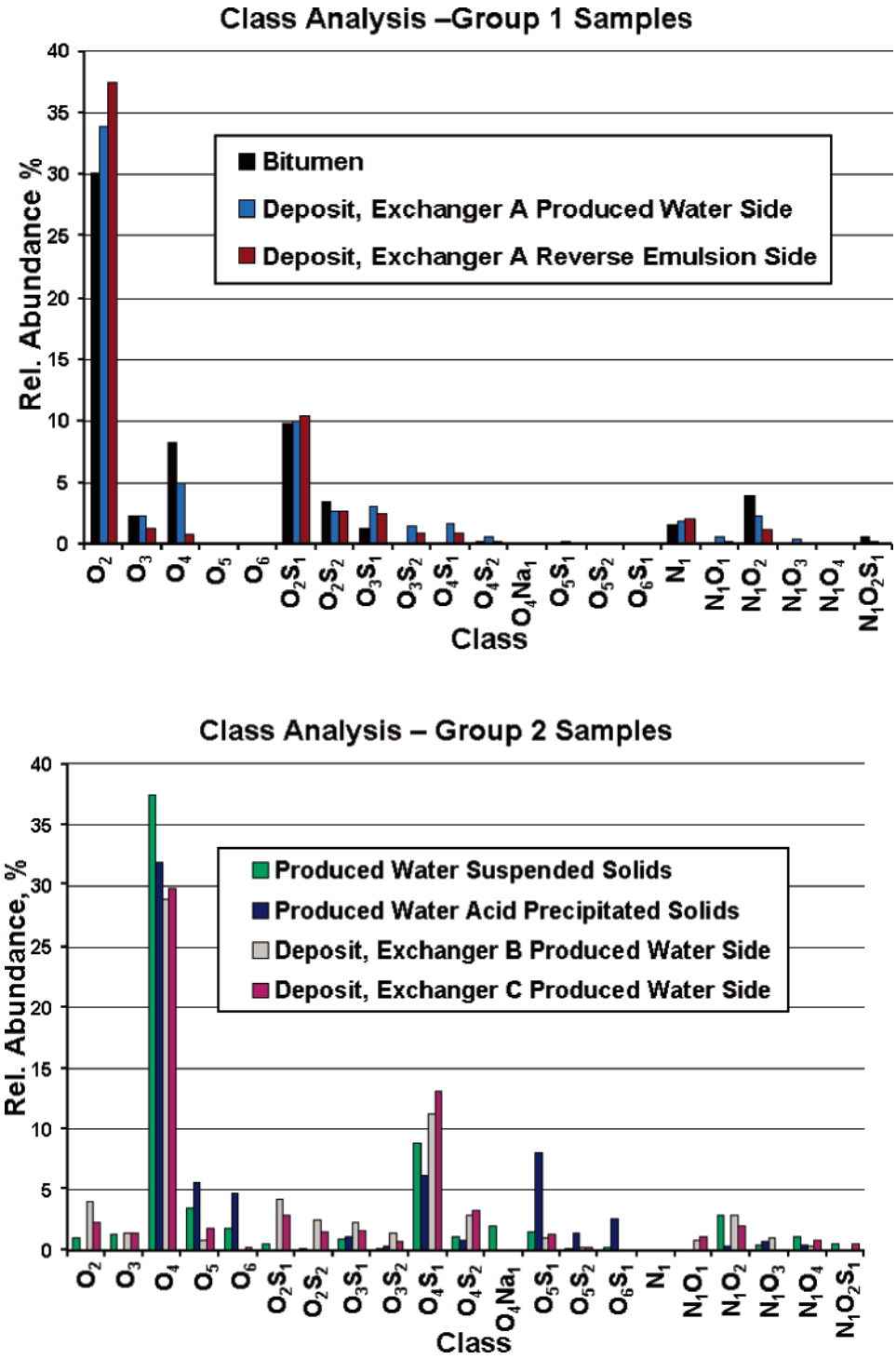

Figure 3. Heteroatom class analysis for (top) the group 1 samples that include the bitumen and the exchanger A reverse emulsion and produced water-side deposit samples and (bottom) the group 2 samples that include the produced water suspended solids and acid-precipitated solids, the exchanger B and C produced water-side deposits. For clarity, only the most abundant half of the observed classes is shown.

particularly along the DBE axis can represent a substantial change in the corresponding molecular structures.

In addition to higher heteroatom content, group 2 samples show higher DBE and a lower carbon number than the group 1 samples, likely because of preferential partitioning of compounds with better solubility and/or dispersion in the produced water flow stream. Both increased DBE (aromaticity) and decreased carbon number (molecular weight) favor improved water solubility.

O_2 Compounds. Abundance-contoured plots of DBE versus the carbon number for O_2 compounds are shown in Figure 4. For the group 1 samples (top of Figure 4), relative abundances peak in two regions: DBE = 3−4, carbon number = 29−30 for the exchanger A produced water-side deposit and DBE = 3−4, carbon number = 35−40 for the exchanger A reverse-emulsion-side deposit. Both areas show a high relative abundance for the bitumen sample. Although group 1 (top of Figure 4) shows primarily species from 2 < DBE < 8 and ∼25−45 carbons, group 2 (Figure 4b) shows a marked shift to higher DBE and a lower carbon number (e.g., primary species at 3 < DBE < 12 and ∼15−27 carbons) and are far less abundant overall. The O_2 species observed in group 2 are largely

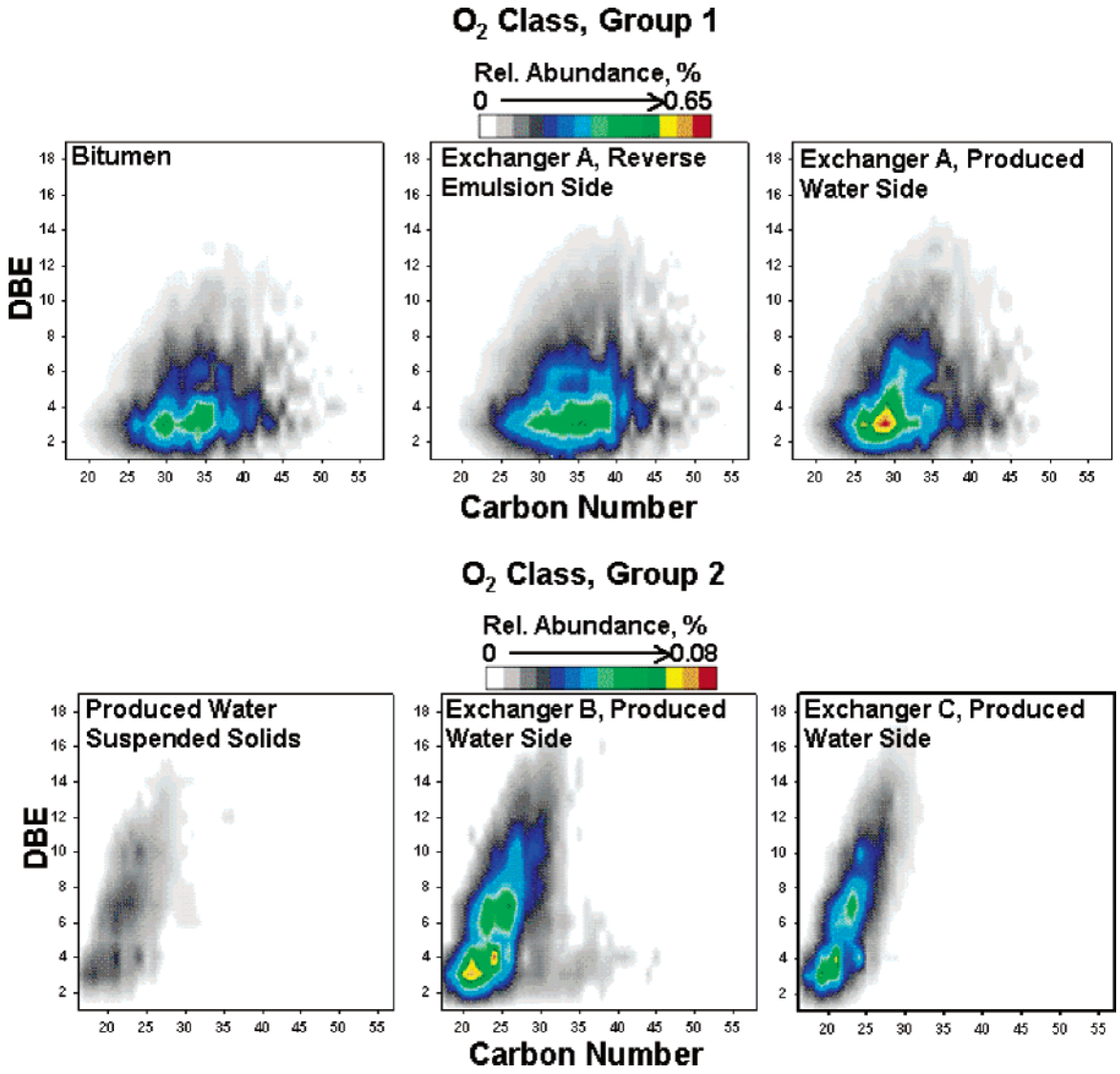

Figure 4. Color-coded isoabundance contour plots of DBE versus the carbon number for O_2 ions from group 1 (top) and group 2 (bottom) samples.

consistent for the produced water suspended solids and exchanger B and C deposits. No O_2 species were observed in the produced water acid-precipitated sample. Interestingly, the exchanger B deposit, which was sampled in closest proximity to the group 1 samples, shows low levels of O_2 compounds in the region of DBE = 3−4 at carbon numbers of ∼30−40, the area of highest abundance for the group 1 samples.

O_4 Compounds. Figure 5 shows abundance-contoured plots of DBE versus the carbon number for observed O_4 compounds. Group 1 (top of Figure 5) shows low-abundance O_4 compounds primarily in the range of 3−5 DBE with carbon numbers from 30−47. The absence of the above O_4 compounds from the exchanger A reverse-emulsion-side deposit may indicate that these species are dissolving or partitioning into the produced water as the reverse-emulsion temperature is increasing through this stage of the facility process and are therefore less prone to deposit. For the exchanger A produced water-side deposit, it is possible that O_4 compounds are more prevalent here (and in exchangers B and C) because of precipitation as the produced water (which may have become saturated) is cooled from 220 °C.

The group 2 samples (bottom of Figure 5) are of interest because the O_4 compounds observed for the produced water suspended solids, the exchanger B deposit, and the exchanger C deposit are quite similar, whereas those for the produced water acid-precipitated sample exhibit substantially higher DBE and a lower carbon number. The lower molecular-weight, more highly condensed O_4 species found in the produced water acid-precipitated sample (which are salts prior to acid precipitation) appear to be well-solubilized in the produced water and thus do not appear to participate in heat-exchanger fouling. The O_4 compounds found in the other group 2 samples are fairly similar to those found in group 1 (especially for the exchanger B deposit) and appear to be significant constituents of the produced water heat-exchanger deposits. The observation of high oxygen content for the deposits is consistent with the results of the bulk analyses presented in part 1. High oxygen content (as determined by semiquantitative energy-dispersive X-ray analysis) has also been reported in a diluted SAGD heat-exchanger deposit analysis.[29]

SO_4 Compounds. Only low-abundance SO_4 compounds were seen in the exchanger A deposits, and none were observed in the produced bitumen. For the exchanger A deposits, the most abundant SO_4 compounds were observed at DBE values from

(29) Wang, S.; Axcell, E.; Bosch, R.; Little, V. Effects of chemical application on antifouling in steam-assisted gravity drainage operations. *Energy Fuels* **2005**, *19*, 1425−1429.

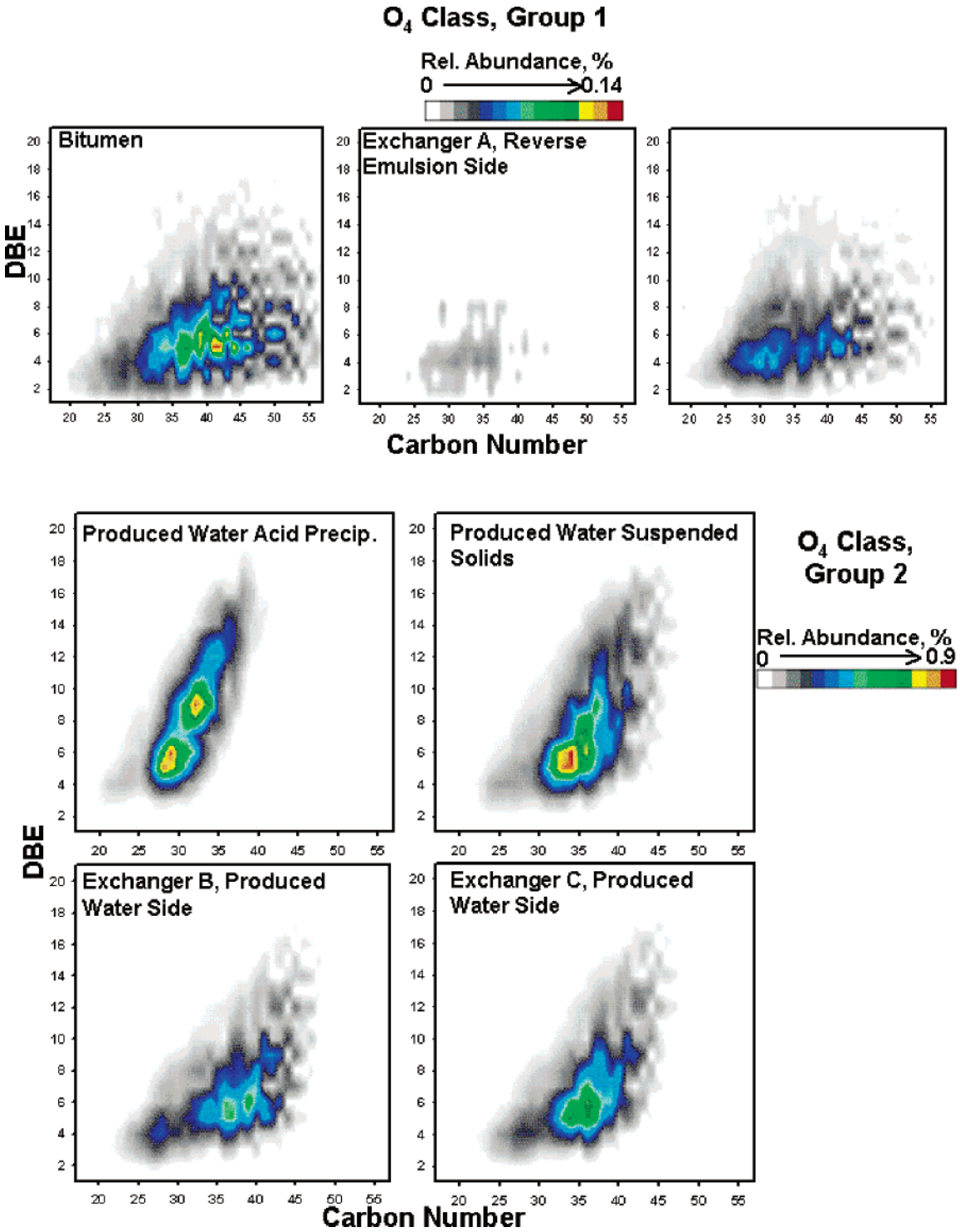

Figure 5. Color-coded isoabundance contour plots of DBE versus the carbon number for O_4 ions from group 1 (top) and group 2 (bottom) samples.

2−12 and carbon numbers of 23−40 (not shown). The highest abundance was observed for both samples at DBE = 5 and a carbon number of 30 at a relative abundance of ~0.025%. Figure 6 shows an abundance-contoured plot of DBE versus the carbon number for group 2 SO_4 compounds. The exchanger B and C deposits are similar, with primary SO_4 compounds in the range of 4 < DBE < 14 and ~33−44 carbons. Except for the produced water acid-precipitated sample, a particularly strong signal was observed for group 2 samples at DBE = 10 and a carbon number of 37 (see tandem mass spectrometry results described below.

The produced water suspended solids and the acid-precipitated samples show more localized distributions than the deposits and have major SO_4 compounds with substantially higher DBE values (~8−16). The major SO_4 compounds for the produced water and the acid-precipitated sample both appear at a DBE value of 10; those in the acid-precipitated sample have ~29−33 carbons, and those in the suspended solids have ~34−41 carbons (i.e., the most abundant SO_4 species in both samples are members of the same homologous series). Therefore, the solubility of major SO_4 compounds in the produced water appears to be influenced by the degree of alkylation, with a

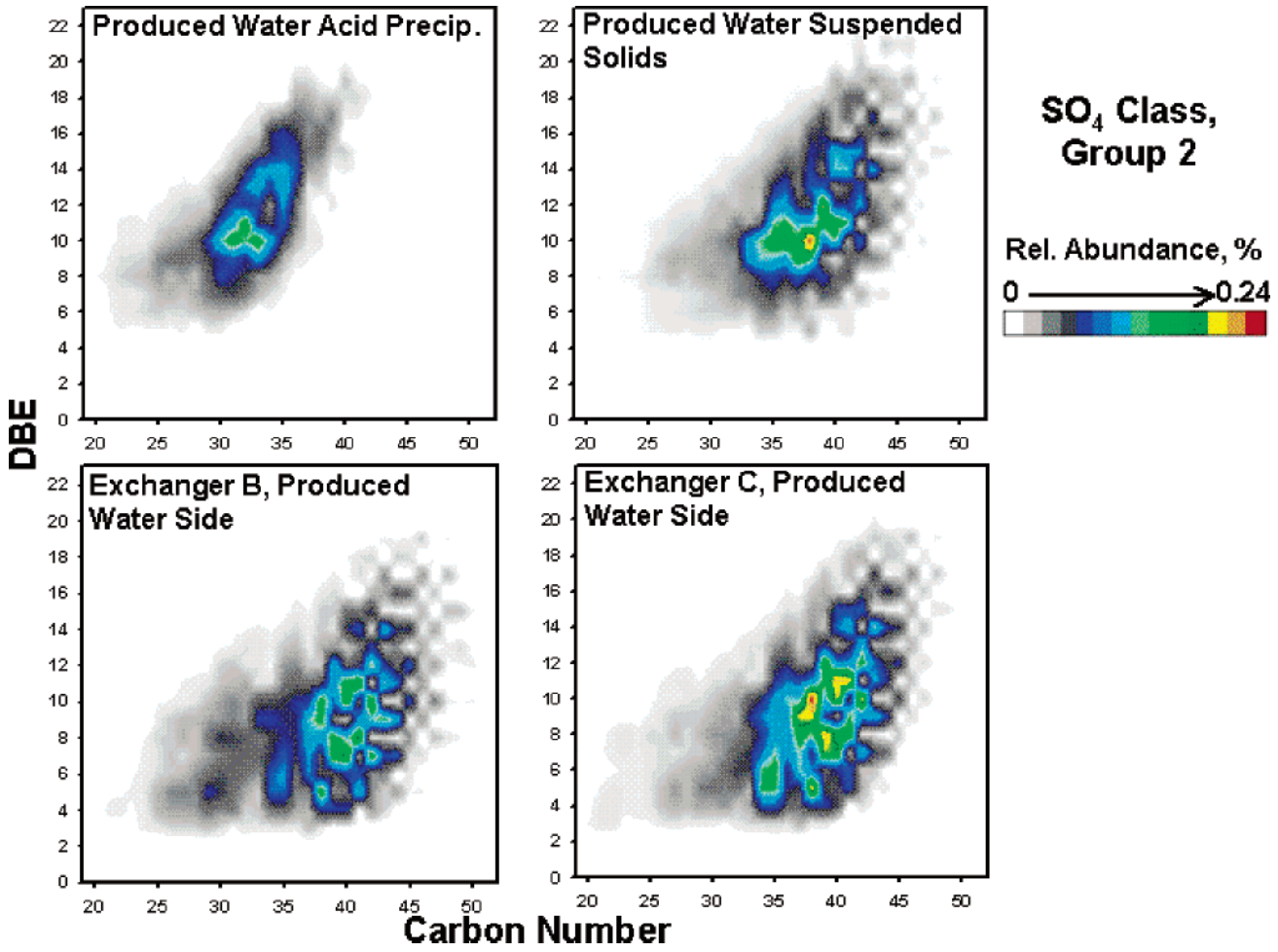

Figure 6. Color-coded isoabundance contour plots of DBE versus the carbon number for SO_4 ions from group 2.

sharp decrease in solubility for SO_4 species that contain more than 34 carbons. Moreover, note that the SO_4 species in the acid-precipitated sample were likely present in the original produced water as sodium salts, which also greatly affect water solubility.

SO_2 Compounds. Abundance-contoured plots of DBE versus the carbon number for SO_2 compounds are shown in Figure 7. For group 1 samples (top of Figure 7), the highest abundance SO_2 species exhibit DBE = 8 and carbon numbers of 25−38. Both exchanger A deposits (reverse emulsion and produced water side) show slightly lower carbon number and higher DBE species than those from bitumen.

The overall abundance of SO_2 compounds observed in the group 2 samples (bottom of Figure 7) is much lower than for group 1. Only very low-abundance SO_2 compounds were observed in the produced water suspended solids sample, and none were found in the produced water acid-precipitated sample. The major exchanger B and C deposit SO_2 compounds display much lower carbon numbers (all less than 30 carbons) across a wider DBE range ($3 < DBE < 9$) than those from group 1.

Acid Salt Compounds. With the exception of one observed class of acid salts (O_4Na, produced water suspended solids sample), no salts were detected by ESI FT-ICR MS. That result is likely due to their insolubility in toluene. FT-IR analyses of the toluene-insoluble portion of the heat-exchanger deposit samples show the presence of acids and acid salts. The results of those analyses are shown in Table 1. Note that acid salts are likely the primary constituents of the "organic" portion of the toluene-insoluble material.

Tandem Mass Spectrometry for Structural Analysis. Infrared multiphoton dissociation was performed for O_4, O_2, SO_4, and SO_2 compounds isolated from the broadband ion populations. Several compounds of highest relative abundance from each class (Figures 4−7) were selected. IR irradiation of the O_4 and SO_4 species produced fragment ions (discussed below), whereas irradiation of O_2 and SO_2 compounds did not yield fragment ions. IRMPD was not performed for compounds in the produced water acid-precipitated sample.

Fragmentation of O_4 Compounds. Figure 8 shows a typical IRMPD fragment ion spectrum, for $C_{36}H_{60}O_4^-$ ions isolated from the exchanger B deposit. Only O_2 fragments are observed. In fact, of the seven O_4 compounds selected from group 2, all behave similarly (i.e., all fragments result from neutral losses of CO_2 and integer numbers of CH_2 groups from the parent compounds). For the three group 2 samples, the O_4 compounds selected for IRMPD analysis ranged from $5 < DBE < 7$ and the most abundant fragments in every case were found at DBE values of 2 or 3. The absence of any O_3 or O_1 fragments indicates that these species are likely dicarboxylic acids.

Similarly, three bitumen, DBE = 5, O_4 compounds were selected for IRMPD analysis, and again, only O_2 fragments were observed, with the most abundant fragments at DBE = 2. Selected O_4 compounds from the other two group 1 samples the exchanger A deposits also yielded only O_2 fragments. However, although those ions showed high-abundance fragments

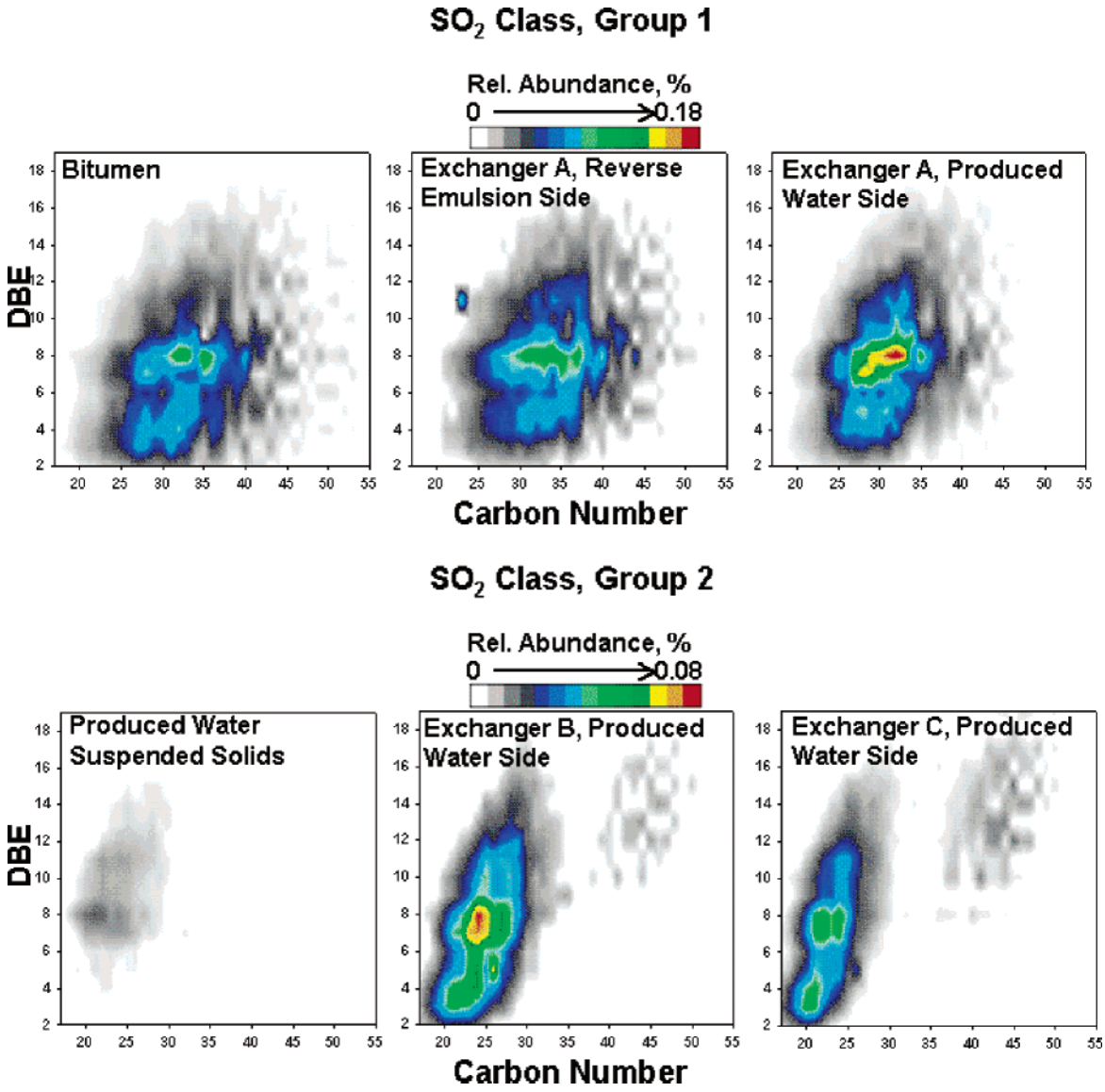

Figure 7. Color-coded isoabundance contour plots of DBE versus the carbon number for SO_2 ions from group 1 (top) and group 2 (bottom).

Table 1. Bulk Analysis of the Toluene-Insoluble Portion of Heat-Exchanger Deposits

exchanger/ location	toluene solubility (wt %)	organics in toluene-insoluble portion (wt %)	FT-IR analysis of toluene-insoluble material
A/reverse emulsion	28	11	Mg-silicates (dominant) with carboxylic acids/acid salts
A/produced water	58	15	Mg-silicates (dominant) with carboxylic acids/acid salts
B/produced water	65	19	Mg-silicates (dominant) with carboxylic acids/acid salts
C/produced water	83	55	carboxylic acids/acid salts (dominant) with Mg-silicates

at DBE = 2, lower abundance (unexplained) fragments were also observed at DBE = 0 and 1.

Fragmentation of SO_4 Compounds. No SO_4 compounds were isolated from group 1 samples because of their low mass spectral peak signal-to-noise ratios. Seven SO_4 compounds were isolated from the broadband electrospray ion populations of three group 2 samples. Figure 9 shows a typical IRMPD fragment ion spectrum for $C_{38}H_{56}SO_4^-$ ions isolated from the exchanger C deposit. The predominant fragment ions are, DBE = 2−9, O_2S species as well as several low-abundance O_2 fragments. All isolated group 2 SO_4 compounds exhibit similar fragmentation behavior. The SO_4 compounds selected for IRMPD analysis ranged from 6 < DBE < 12 and show only fragments formed by neutral losses of CO_2/CO_2S and integer numbers of CH_2 groups from the precursor ions, suggesting that the group 2 SO_4 compounds are dicarboxylic acids with thiophenic core structures.

Conclusion

In this work, we have detailed the organic acid content of seven samples from an inverted SAGD processing facility. (−) ESI FT-ICR MS provides sufficient resolving power to observe several thousand chemically unique compounds for each sample, and sub-ppm mass accuracy enables molecular formula assignment for the observed ion signals.

Heteroatom class analysis based on the molecular formula assignments reveals two groups within the seven samples. One group consists of reverse-emulsion-type deposits and the

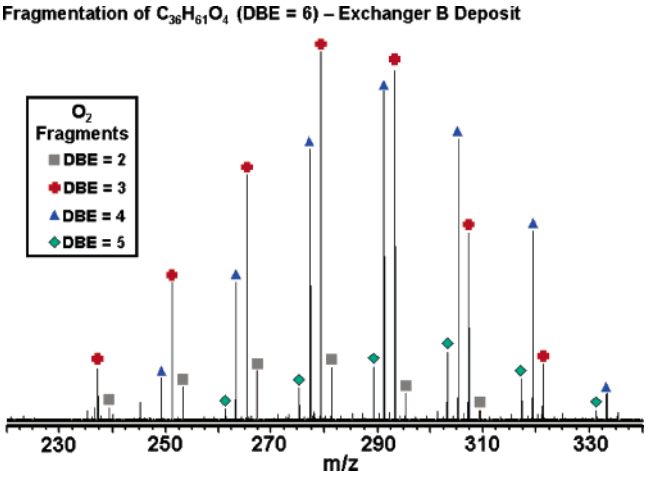

Figure 8. Fragment ion mass spectrum from $C_{36}H_{61}O_4^-$ precursor ions from the exchanger B deposit. Note that only O_2 fragments with $2 < DBE < 5$ and various degrees of alkylation are observed.

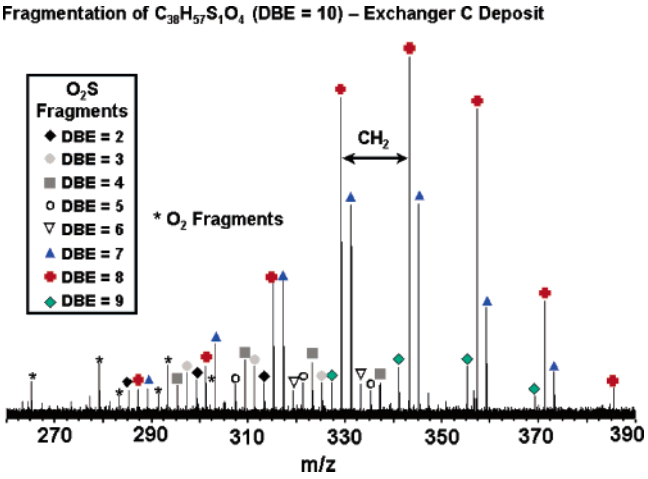

Figure 9. Fragment ion mass spectrum from $C_{38}H_{57}SO_4^-$ precursor ions from the exchanger C deposit. Note that predominantly SO_2 fragments with $2 < DBE < 9$ and various degrees of alkylation are observed. Some O_2 fragments were observed as well at $3 < DBE < 5$.

produced bitumen and shows high levels of O_2, O_2S, and N_1 compounds. The second group originates from the produced water, following high-temperature separation of the bitumen from the reverse emulsion, and from subsequent deposits on the produced water heat exchangers. This second sample group shows high levels of O_4 compounds, SO_4 compounds, and other compounds with high heteroatom content.

Abundance-contoured plots of DBE versus the carbon number afford convenient visualization of elemental composition patterns. The highly abundant O_2 compounds in group 1 samples are lower in DBE and higher in the carbon number than the much lower abundance O_2 compounds from group 2. Attempts to fragment O_2 compounds from all samples yielded no fragment ions.

Only low-abundance O_4 compounds were present in reverse-emulsion group 1. The extremely high abundance of O_4 compounds in the produced water deposits and samples indicates that those species are major constituents of the produced water heat-exchanger deposits. Fragmentation of O_4 compounds from all samples indicates that the observed compounds are dicarboxylic acids.

SO_4 compounds are also observed in high abundance for the group 2 samples and appear as major constituents of the produced water deposits. The SO_4 compounds observed in the produced water suspended solids and the acid-precipitated sample exhibit higher DBE than those of the produced water heat-exchanger deposits. IR fragmentation of selected SO_4 compounds suggests dicarboxylic acid/thiophenic sulfur structures.

Although heat-exchanger fouling is a severe operational problem in SAGD processes, little has been known about the fouling process. Deposit formation proceeds through a complex mechanism that encompasses the fluid dynamics, phase behavior, and physical carryover of material in the process flow stream. Therefore, the first logical step for understanding deposition formation is to characterize the species that have deposited. In this work, a systematic evaluation of deposit and fluid samples collected from different locations in one inverted SAGD facility provides insight into the composition and chemical structures of some of the dominant species that contribute to fouling. In addition, we observe the role of the chemical structure in partitioning these species (originating from bitumen) into the produced water flow stream and their subsequent deposition from the produced water flow stream as process conditions change.

Acknowledgment. This work was supported by the NSF National High Field FT-ICR Facility (DMR 00-84173) at the National High Magnetic Field Laboratory, Florida State University, Tallahassee, FL.

EF0601115